Biosensors and Bioelectronics 208 (2022) 114193

Contents lists available at ScienceDirect

Biosensors and Bioelectronics

journal homepage: www.elsevier.com/locate/bios

Nanoplasmonic multiplex biosensing for COVID-19 vaccines

Riccardo Funari [a,b,**], Hidehiro Fukuyama [c,d,e], Amy Q. Shen [a,*]

[a] Micro/Bio/Nanofluidics Unit, Okinawa Institute of Science and Technology Graduate University, 1919-1 Tancha, Onna-son, Okinawa, 904-0495, Japan
[b] Dipartimento di Fisica "M. Merlin", Università degli Studi di Bari "Aldo Moro", Bari, 70125, Italy
[c] Laboratory for Lymphocyte Differentiations, RIKEN Center for Integrative Medical Sciences (IMS), Yokohama, Kanagawa, 230-0045, Japan
[d] Near-InfraRed Photo-Immunotherapy Research Institute, Kansai Medical University, Hirakata, Osaka, 573-1010, Japan
[e] INSERM EST, Strasbourg Cedex 2, 67037, France

ARTICLE INFO

Keywords:
SARS-CoV-2
COVID-19 vaccines
Serum antibody
Mono-biotinylation
LSPR
Multiplexing
Gold electrodeposition

ABSTRACT

The ongoing emergence of severe acute respiratory syndrome caused by the new coronavirus (SARS-CoV-2) variants requires swift actions in identifying specific antigens and optimizing vaccine development to maximize the humoral response of the patient. Measuring the specificity and the amount of antibody produced by the host immune system with high throughput and accuracy is critical to develop timely diagnostics and therapeutic strategies. Motivated by finding an easy-to-use and cost-effective alternative to existing serological methodologies for multiplex analysis, we develop a proof-of-concept multiplex nanoplasmonic biosensor to capture the humoral response in serums against multiple antigens. Nanoplasmonic sensing relies on the wavelength shift of the localized surface plasmon resonance (LSPR) peak of gold nanostructures upon binding interactions between the antibodies and the immobilized antigens. Here the antigens are first immobilized on different sensing areas by using a mono-biotinylation system based on the high affinity interaction between biotin and streptavidin. We then validate the multiplex platform by detecting the presence of 3 monoclonal antibodies against 3 antigens (2 different hemagglutinins (HAs) from influenza viruses, and the SARS-CoV-2 Spike RBD (receptor binding domain)). We also measure the humoral response in murine sera collected before and after its immunization with the SARS-CoV-2 Spike protein, in good agreement with the results obtained by the ELISA assay. Our nanoplasmonic assays have successfully demonstrated multiple serum antibody profiling, which can be further integrated with microfluidics as an effective high throughput screening platform in future studies for the ongoing SARS-CoV-2 vaccine development.

1. Introduction

In the pandemic of severe acute respiratory syndrome caused by the new coronavirus (SARS-CoV-2) (Wu et al., 2020; Žižek, 2020), the rapid detection of infected population and vaccine development are both required to control the disease (Chauhan et al., 2020; Dutta et al., 2020; Zhai et al., 2020). Unfortunately the emerging virus variants make the pandemic situation very challenging (Koyama et al., 2020). The profiling of specificity and quantity of the serum antibody is highly informative and has served pivotal roles in developing individualized diagnostics and therapeutics strategies (Amanat et al., 2020; Bai et al., 2020; Burbelo et al., 2020; Casadevall and Pirofski, 2020; Guo et al., 2020; Liu et al., 2020; Zhao et al., 2020; Drobysh et al., 2022; Bian et al., 2022), targeting a broad range of infectious diseases such as influenza (Fukuyama et al., 2020). In particular, antibody detection and quantification is essential to determine the SARS-CoV-2 antibody prevalence and monitor the temporal immune responses in vaccine recipients (Valera et al., 2021; Theel et al., 2020). In the era of epidemiological surveillance, point-of-care (POC) devices possessing the sensitivity and specificity comparable to the standard laboratory instruments can support these efforts, offer unique advantages in portability, on-site analysis capability, reduced sample processing volume and time, and cost effectiveness (Valera et al., 2021). Specifically, miniaturized and multiplexed detection systems only need minute sample volumes with the

* Corresponding author.
** Corresponding author. Micro/Bio/Nanofluidics Unit, Okinawa Institute of Science and Technology Graduate University, 1919-1 Tancha, Onna-son, Okinawa, 904-0495, Japan.
E-mail addresses: riccardo.funari@uniba.it (R. Funari), hiehiro.fukuyama@gmail.com (H. Fukuyama), amy.shen@oist.jp (A.Q. Shen).
URL: https://groups.oist.jp/mbnu (A.Q. Shen).

https://doi.org/10.1016/j.bios.2022.114193
Received 16 September 2021; Received in revised form 11 March 2022; Accepted 14 March 2022
Available online 31 March 2022

possibility of identifying the circulating variants rapidly in real time (Zhu et al., 2020; Zhang et al., 2021; Antiochia, 2021; Orlov et al., 2020; Mas et al., 2020; Hartanto et al., 2020; Heaney et al., 2021; Grossberg et al., 2021; Bray et al., 2021; Bhalla et al., 2020).

Several COVID serological tests have received the Emergency Use Authorization (EUA) from FDA since early 2020 (U.S. Food and Drug Administration, 2020). Among them, enzyme linked immunosorbent assays (ELISA), chemiluminescent immunoassays, and neutralization assays (Muruato et al., 2020) are reliable but laborious and time-consuming (John Hopkins Center for Health Security, 2020). Lateral flow assays can provide more rapid diagnostics (i.e, 10–30 min) and are user-friendly, but the results are only qualitative with low accuracy (Carter et al., 2020; Udugama et al., 2020; John Hopkins Center for Health Security, 2020).

We have recently developed a localized surface plasmon resonance (LSPR) detection platform, to accurately measure the concentration of COVID-19 antibodies present in diluted blood plasma with high sensitivity and speed (Funari et al., 2020). The LSPR sensing principle relies on the local refractive index (RI) changes around the metal nanostructures due to the biomolecule binding events (i.e., antigen-antibody binding). This leads to a wavelength shift of the LSPR peak of the metal nanostructures, which is directly proportional to the target antibody concentration (Willets and Van Duyne, 2007; Mayer and Hafner, 2011). One major advantage of LSPR-based detection is that the short decay length of the electromagnetic field in localized surface plasmons greatly reduces interfering effects from the bulk solution, which is desirable when analyzing complex samples such as blood or serum (Szunerits and Boukherroub, 2012). In this work, we extend the singleplex nanoplasmonic assay design described above to develop a proof-of-concept nanoplasmonic multiplex antibody detection platform to capture the humoral responses against 3 specific antigens in real sera samples, which is important and timely considering the ongoing SARS-CoV-2 pandemic and related vaccine development. Nanoplasmonic sensors have been used for the sensitive multiplex detection of biomolecules such as serum cytokines (Chen et al., 2015), cancer biomarkers (Lee et al., 2015) and Alzheimer biomarkers, and more recently SARS-CoV-2 genes (Wu et al., 2022), proteins and antibodies (Masterson et al., 2021). However, most of these approaches require laborious and complex fabrication procedures which limit their potential utilities in commercial devices. Our nanoplasmonic platform requires a simple and fast two-step fabrication process involving maskless lithography and gold electrodeposition (ED), enabling fabrication of 3 × 3 arrays of sensing spots containing gold nanospikes. We first immobilize 3 different antigens (receptor binding domain (RBD) of spike protein from SARS-CoV-2, and two different hemagglutinins (HAs) from influenza viruses) on 3 different columns of the array. Next, 3 representative monoclonal antibodies (mAb) at 10 ng/mL (clinically relevant concentration for standard proteins) with different selectivity are deposited to the 3 corresponding sensing spots. The wavelength shift is measured to verify the binding activity between the antigen and antibody pairs. To validate the detection of serum antibody against the Spike RBD, we analyze the murine sera collected before and after the immunization with the full length of SARS-CoV-2 Spike protein. The sensor response profile shows a clear signal specifically against the Spike RBD after the immunization, verifying the production of antibodies from the murine model by vaccination. Several sensing technologies have been used to quantify anti-SARS-CoV-2 antibodies in serum. Optical biosensors, such as colorimetric (Lee et al., 2022), luminescent (Elledge et al., 2021) and fluorescence (Rodriguez-Moncayo et al., 2021; Cady et al., 2021; Duan et al., 2022) based biosensors have proven to be easily integrable with microfluidic systems, thus greatly reducing the assay time and the required sample volume, with detection limits on the order of 10 pM. However, these systems are not label-free, and the biomarker quantification is performed through extensive and complex image analysis. On the other hand, electrochemical sensors provide better performances with direct electrical signals (i.e., current or impedance changes) that require minimal signal processing. For example, graphene-based electrochemical sensors achieved detection limits on the order of ≈10 fM for anti-SARS-CoV-2 antibodies (Torrente-Rodríguez et al., 2020; Ali et al., 2021; Yakoh et al., 2021; Mattioli et al., 2022; Oliveira et al., 2022). However, the fabrication procedures are sometimes complex, and require high spatial resolution and temperature control. Concerning plasmonic sensors, Masterson et al. (2021) achieved excellent detection limits in the aM-fM range for anti-SARS-CoV-2 antibodies with gold nanoplasmonic structures deposited on glass slides, integrated in commercial ELISA plates. But the device fabrication required a complex and laborious procedure involving multiple phases with strict temperature control. In comparison with these sensing methodologies, our sensing platform offers label-free detection of the humoral response with easy, rapid and low-cost two-steps fabrication procedure involving only maskless lithography and electrodeposition, both of which can be performed at room temperature, enabling the fabrication of sample batches in less than 1 h. Even though the sensitivity of our device (pM range) is lower than that of some of the techniques mentioned above, it still proves to be sensitive enough to detect anti-SARS-CoV-2 antibody in real samples.

2. Materials and methods

The detailed description of the fabrication of the gold nanospike arrays, the morphological characterization of the gold nanospikes by scanning electron microscopy, the optical setup, the gold functionalization and sensing protocol, and the ELISA assay protocol, are all reported in the Supplementary Material.

2.1. Chemicals and biological materials

Most chemicals used in this work were purchased from Sigma Aldrich, Japan unless stated otherwise. Glycerol, acetone, isopropanol, ethylene glycol, and MilliQ® water (Millipore, Japan) were used for the sensitivity measurements and sample preparations. Gold (III) chloride trihydrate (520918), lead (II) acetate trihydrate (316512), bovine serum albumin (BSA, A2153), IHC Select Secondary Goat anti-Mouse IgG, anti-Rabbit IgG, biotinylated (20775) and phosphate buffered saline (PBS) tablets (P4417), 11-mercaptoundecanoic acid (450561) and 6-mercapto-1-hexanol (725226) are used for the nanostructure fabrication and surface functionalization. N-hydroxysuccinimide (NHS, 24500) and 1-ethyl-3-(3-dimethylaminopropyl)carbodiimide hydrochloride (EDC, 22980) were purchased from Thermo Scientific, Japan for self-assembled monolayer (SAM) activation to covalently immobilize the streptavidin.

Recombinant extracellular domain of hemagglutinins (HA) from A/California/7/2009(X-179A)(H1N1)pdm09 (H1) or A/Okuda/1957 (H2N2) (H2) was fused with T4 fibritin foldon trimerization domain, biotinylatable AviTag™, and a hexahistidine tag. Recombinant extracellular domain of Spike protein from SARS-CoV-2 Wuhan, QHD43416.1 (VG40589-UT, Sino Biological) was fused with T4 fibritin foldon trimerization domain, TEV protease (Tobacco Etch Virus nuclear-inclusion-a endopeptidase) cleavage site, AviTag™, and a hexahistidine tag(full-length). Recombinant Spike RBD (319–591 a.a.) was fused with TEV protease cleavage site and AviTag™, and a hexahistidine tag (named as Spike). These recombinant proteins were produced in Expi293™cells by co-expression of BirA (Addgene 64395) and purified using Nickel column. C179 (Okuno et al., 1993) and NSP2 (Matsuzaki et al., 2014) were produced from hybridomas gifted from Drs. Okuno (OIPH) and Takahashi (NIID), respectively. Recombinant C121 antibody was gifted from Dr. Shirouzu (RIKEN). Sera were obtained from C57BL/6JJcl mice (CLEA Japan, Inc) before immunization and at 4 weeks after immunization of recombinant full-length Spike protein.

2.2. Gold electrodeposition and surface patterning

Patterned arrays of Au nanospikes (schematic shown in Fig. 1a) were fabricated with a two-step process. The surface of a 15 mm × 15 mm gold coated glass slide was first coated by a 2 μm thick polymer film, and then patterned using a maskless lithography system. The exposed area consists of a 3 × 3 array of 2 mm circular spots (zoomed-in image in Fig. 1a) on which the gold (Au) nanospikes were next fabricated by

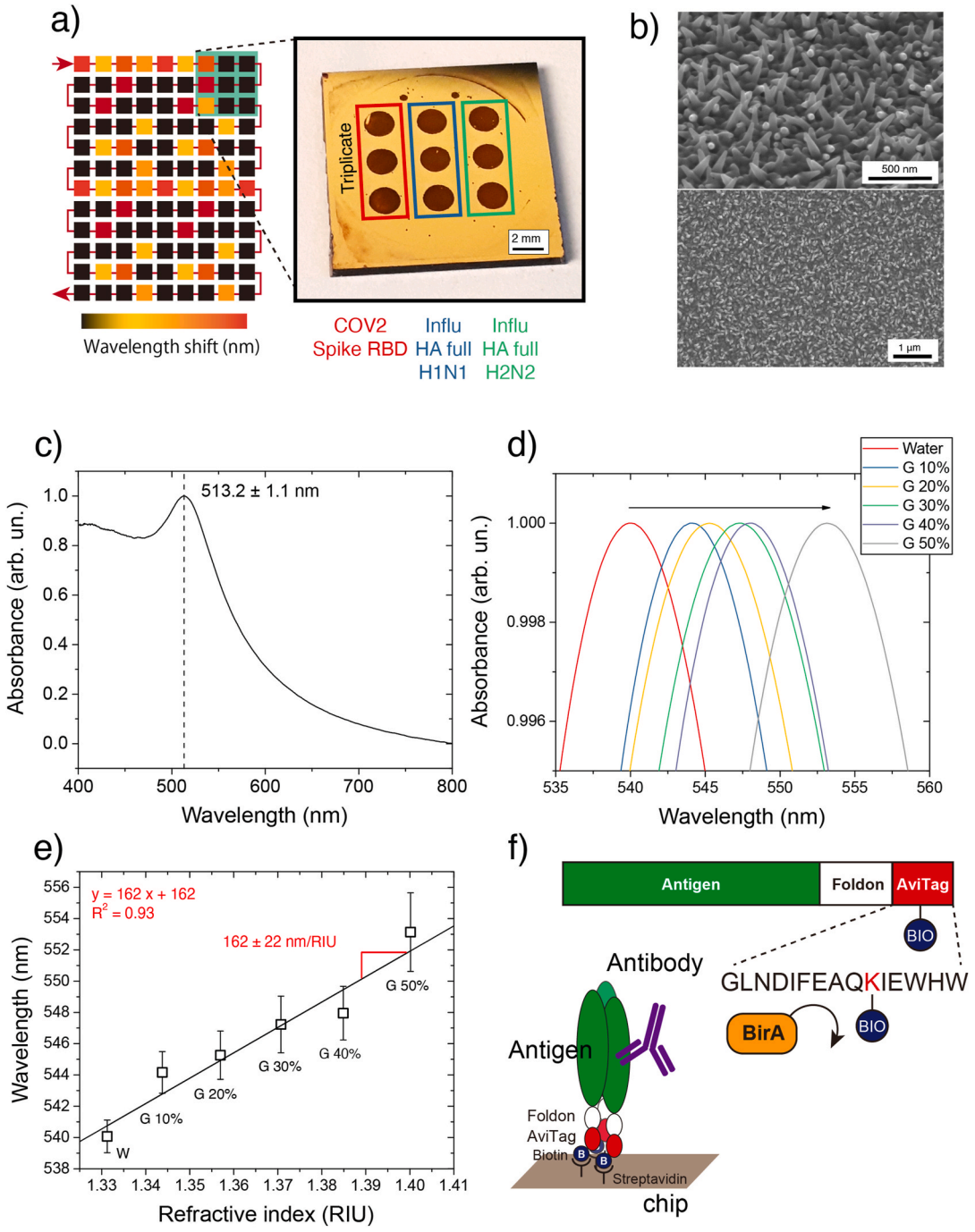

Fig. 1. (a) Schematic design principle of our multiplex bioassay platform and a photo snapshot of the gold coated glass slide containing 3 × 3 spot arrays. The reddish circular spots represent the portion of the substrate covered by the Au nanospikes generated by ED. Each vertical array is functionalized with a different antigen in triplicate, illustrated in red, blue, and green boxes. The two small dots on top of the array serve as reference locations for fabrication purposes. (b) SEM images of Au nanospikes (top) side view, tilted (40°) and 100,000, (bottom) top view, 30,000. (c) Normalized average absorbance spectrum for Au nanospikes. The plot represents the average spectra collected on all 9 spots with 3 different substrates. (d) Absorption spectra resulting from the exposure of gold nanospikes to 6 aqueous solutions with different RIs: water (W) and water/glycerol (G) mixtures with varying concentrations (10 to 50% w/w). The black arrow highlights the red shift in the plasmonic peak due to the increase in the RI of the solution. (e) The RI sensitivity of our multiplex substrate is calculated by linear regression from LSPR peak shifts recorded for water and glycerol mixtures shown in (d). Each data point corresponds to the average data from triplicate experiments, with the error bars denoting the standard deviation. (f) AviTag™-mediated antigen preparation. Bacterial biotinylation enzyme, BirA, recognizes the 15-a.a. sequence and covalently bonds a biotin to the lysine in the sequence. Antigen is trimerized by foldon as the Spike in the native condition. This mono-biotinylated antigen is immobilized on the streptavidin-coated sensing spots. (For interpretation of the references to color in this figure legend, the reader is referred to the Web version of this article.)

electrodeposition (ED). Once the ED process was completed, the Au nanospike covered glass substrate was washed in acetone (ACE), isopropanol (IPA) and MilliQ® water to remove the photoresist, followed by a gentle stream of nitrogen for drying before the surface functionalization steps. Note that all the results shown in this work are based on the optimized ED protocol (voltage of -1.5 V for 360 s) which provides the most regular and uniform Au nanospikes (SEM image in Fig. 1b), and display the strongest light absorption at ≈ 513 nm (see absorption spectrum in Fig. 1c). Details of the ED process can be found in the Supplementary Material.

3. Results and discussion

For proof-of-concept studies, we restrict our attention to validate the multiplex antibody-antigen detection scheme (see Fig. 1a) without integrating microfluidics in the assay.

3.1. Nanoplasmonic properties of sensing arrays

The RI (refractive index) sensitivity of the sensing arrays covered by Au nanospikes was calculated by measuring the wavelength shift in the LSPR peak position when the gold nanospike covered substrate was incubated with aqueous glycerol mixtures with different glycerol concentrations (10–50% w/w, corresponding to different RI). The spectra of the gold nanospikes exposed to these solutions are shown in Fig. 1d. The LSPR peak shift versus the RI of the solution is plotted and the RI sensitivity of Au nanospike-based sensor substrate (the slope of the linear fit shown in Fig. 1e) was calculated to be 162 nm/RIU, which is comparable with the refractive index sensitivity of gold nanostructures reported in literature (Chen et al., 2008; Kurt et al., 2021). This value is slightly smaller than those reported in our previous work (Funari et al., 2020) (i.e., 183 nm/RIU) due to slightly modified ED process to accommodate the surface patterning on the gold slide for multiplex assays. However, this small change does not affect the detection procedure and results.

3.2. Surface functionalization and immobilization of mono-biotinylated proteins

Taking advantage of the strong affinity interaction between streptavidin and biotin, we employ a well-established AviTag™-mediated ectopic mono-biotinylation system to functionalize the sensor surface. As shown in the top panel of Fig. 1f, the antigen is produced by mammalian cells expressing bacterial biotinylation enzyme, BirA, so that the enzyme links a single biotin to the tagged region of the protein, which is far from the antigenic domain of the protein. This allows us to preserve the original epitope of the antigen (bottom panel of Fig. 1f), therefore, minimizing the false negative results in the antibody detection. This reliable immobilization procedure can be easily tuned for different antigens as long as they are biotinylated, thus enabling flexible and general detection scheme. We further highlight the key advantages of using AviTag™-mediated ectopic mono-biotinylation system as follows: (1) Due to the high affinity of biotin-avidin interaction, non-specific binding can be minimized. Moreover, streptavidin has four biotin binding sites for multivalency. This leads to enhanced specificity and sensitivity for our multiplexed assay; (2) The ectopic mono-biotinylation avoids the biotinylation in the internal sequence of the antigen, so the native protein shape of the antigen on the chip can be preserved; (3) The mono-biotinylation establishes the biotin-antigen at 1:1 molecular ratio. This allows us to easily control the quantity of antigens on the chip without labor-intensive process to optimize antigen immobilization individually for different antigens in the multiplex format (e.g., incubation time, concentration, etc.).

Each stage of the functionalization of gold nanospike was then validated by measuring the wavelength shift of the LSPR peak position on the substrate at each step of the protocol after washing the substrate with MilliQ water to remove any salt residues (details in Section S4 and Fig. S1a). First, the Au nanopsikes were coated with an alkyl thiol SAM consisting of MCH and MUA. The carboxylic groups of the MUA were activated using the EDC/NHS chemistry and the straptavidin molecules were covalently bonded by their surface amines. Next, the Au nanospike covered substrate was incubated with biotinylated proteins, which were captured by the immobilized streptavidin on the biotin label. Since all the immobilized proteins used in this work are based on biotin/streptavidin biomolecular interaction, we calibrated the functionalization of the sensor surface by using a standard biotinylated protein mixture (IgG). This immobilization procedure does not depend on the size or the nature of the antigen, but only on the presence of the biotin label. Therefore, the protocol derived from using the reference biotinylated IgG can be extended to other biotinylated antigens, which might not be readily available or more expensive (i.e., COVID-19 related antigens). The immobilization concentration of biotinylated antigen was determined by measuring the sensor response at different concentrations of biotinylated IgG. The dose-response curve (see Fig. S2b in the Supplementary Material) shows that the sensor surface is saturated with biotynilated proteins at 5 μg/mL. Therefore, this protein concentration is used for the immobilization of all the antigens (with smaller molecular weights) used in this study. More details can be found in the Supplementary Material.

3.3. Validation of multiplex nanoplasmonic sensing

After functionalizing streptavidin on the Au nanoplasmonic substrate, we immobilized mono-biotinylated Spike RBD, H1 and H2 antigens on the 3 × 3 sensing arrays (Fig. 1a). The sensor array was then incubated with 10 ng/mL solution of 3 representative monoclonal antibodies C121, C179 and NSP2 (see Fig. 2a). Briefly, C121 is an antibody isolated from convalescent plasma from a COVID-19 patient (Robbiani et al., 2020). The antibody C121 binds specifically to the RBD of the Spike protein. C179 is a broadly-neutralizing antibody against influenza viruses (Okuno et al., 1993). This antibody recognizes the structural epitope comprised of both HA1 and HA2 domains in the hemagglutinin stem region (Dreyfus et al., 2013). Since the region is evolutionary conserved, the antibody C179 can bind HAs of several strains of group 1 influenza viruses such as H1N1 and H2N2. In contrast, antibody NSP2 only binds HAs from influenza H1N1 2009 pandemic strains (Matsuzaki et al., 2014). We further highlight that with conventional random cross-linking method for antigen immobilization, C179 cannot recognize the HA antigen. Thus, we chose monoclonal antibodies with AviTag™-mediated ectopic mono-biotinylation system for controlled studies.

Using our multiplex sensor platform, C121 displayed a robust wavelength shift of ~ 4.0 nm on the sensing spots where RBD was immobilized (red data in Fig. 2b), consistent with the fact that C121 is specific to the Spike RBD. Since C121 does not bind the H1 and H2 antigens, the wavelength shifts on spots functionalized with H1 and H2 antigens showed very negligible signals (~ 0.3 nm). Similarly, C179 (blue bars) and NSP2 (green bars) displayed different selectivity with the 3 antigens of interests. C179 is specific against both H1 and H2 (~ 2.7 nm and ~ 2.0 nm respectively), while NSP2 binds only the H1 antigen (~ 4.0 nm). The wavelength shifts measured for these 3 mAbs (data shown in Fig. 2b) are consistent with the characteristics of the 3 mAbs with respect to Spike, H1, and H2 antigens (Fig. 2a). These results validated the sensing procedure we developed and demonstrated that our LSPR-based multiplex platform could identify the presence of specific antibodies in the sample of interest. More importantly, by using the same fabrication and sensing protocols, the 3 × 3 sensing arrays can be easily expanded on the same chip to achieve higher throughput.

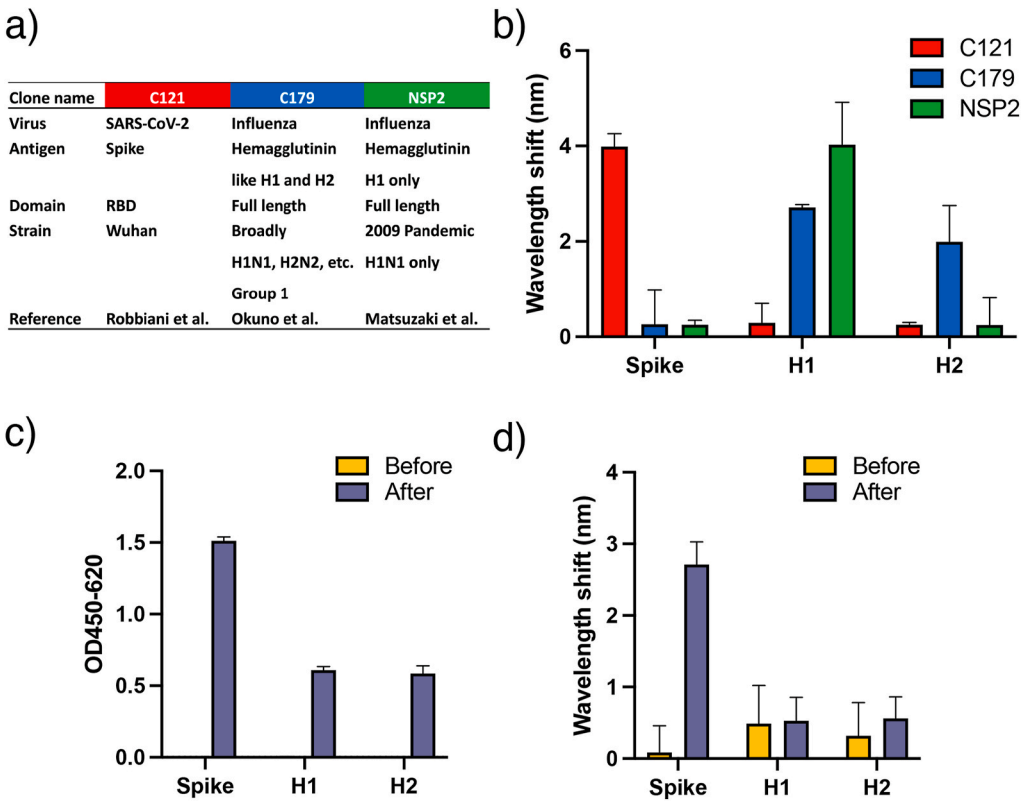

Fig. 2. (a) Monoclonal antibodies used in this study. (b) LSPR responses against 10 ng/mL of C121 (red), C179 (blue) and NSP2 (green) mAbs in PBS. (c) ELISA outputs for murine sera collected before and after the immunization with the SARS-CoV-2 Spike protein. The values of the optical density (OD) of 450 nm wavelength subtracted by the background at 620 nm wavelength are plotted for Spike, H1 and H2 antigens. (d) LSPR responses against 1:100 diluted murine sera of before and after the immunization with the SARS-CoV-2 Spike protein. Each data point corresponds to the average data from triplicate experiments, with the error bars denoting the standard deviation. (For interpretation of the references to color in this figure legend, the reader is referred to the Web version of this article.)

3.4. Evaluation of multiplex nanoplasmonic sensing for murine vaccination model

To evaluate our murine vaccination model, we first immunized mice with the full-length Spike protein containing the foldon-AviTag™-hexahistidine tag fragment. The serum contains antibodies against the Spike RBD and the foldon-AviTag™-hexahistidine tag fragment. The serum samples were obtained from mice before and after being immunized with the full-length spike protein and subjected to both conventional ELISA and our multiplex LSPR-based assays.

In the ELISA experiment (Fig. 2c), we determined the optical density (OD) of colorimetric reaction products by subtracting readings at 620 nm (background) from the readings at 450 nm. As expected, the serum antibody level against Spike RBD (Spike) was significantly raised after immunization (purple) but not before immunization (yellow). However, the increased antibody concentration in the serum after immunization only reacted with H1 and H2 at the minimum level. This negligible increase from the level of non-immunized samples is most likely due to the portion of the serum antibodies against the foldon-AviTag™-hexahistidine tag fragments present in the HA antigens (H1 and H2), which is commonly used in both the immunized antigen and the detection antigens.

Next we used our multiplex nanoplasmonic platform to quantify antibodies in sera. The sensor responses against the pre-and post-immunization sera are shown in Fig. 2d. Since the mice were not exposed to any of the antigens in the pre-immunization sample (yellow bars), the sensor responses (i.e., the wavelength shifts < 1 nm) fall within the experimental error. If the mice were immunized with the Spike protein, their immune system response would be revealed by producing large amounts of specific antibodies. Indeed, the response profile for the serum of the immunized animal (purple data) displayed a significant wavelength shift against the Spike RBD, but only showing negligible shifts (comparable with the background), for H1 and H2 antigens. The detailed wavelength shifts for tested samples are reported in Table 1. Note that specific response against the Spike antigen in the sera (2.7 nm) is smaller than that achieved by the C121 mAb (4.0 nm). This is reasonable since mAbs have higher affinity for selected targets, while humoral response in sera is due to polyclonal antibodies (i.e., antibodies secreted by different memory B cells), which have different affinities for the antigen (Murphy and Weaver, 2016). Nevertheless, the comparison of our nanoplasmonic response against the 3 antigens is in good agreement with those obtained by the ELISA assay (Fig. 2c), thus validating the performances of our multiplex nanoplasmonic platform even in complex biological fluids such as blood serum, which contains biomolecules like hormones, globulins, etc., that can potentially induce non-specific responses (Szunerits and Boukherroub, 2012).

Table 1
LSPR wavelength shifts used in Fig. 2b and d. The larger shifts (highlighted in bold) correspond to significant amounts of specific antibodies which bond to the immobilized antigens.

Wavelength shift due to antibody detection (nm)			
	Spike	H1	H2
C121	**4.0 ± 0.3**	0.3 ± 0.4	0.3 ± 0.1
C179	0.3 ± 0.7	**2.7 ± 0.1**	**2.0 ± 0.8**
NSP2	0.3 ± 0.1	**4.0 ± 0.9**	0.2 ± 0.6
Serum before immunization	0.1 ± 0.4	0.5 ± 0.5	0.3 ± 0.5
Serum after immunization	**2.7 ± 0.3**	0.5 ± 0.3	0.6 ± 0.3

Nanoplasmonic biosensors based on gold nanostructures have also been used for the detection of important biomolecules including COVID-19 biomarkers (Lee et al., 2015; Chen et al., 2015; Kim et al., 2018; Masterson et al., 2021). Some of these approaches provide high sensitivity and excellent limit of detection, but suffer from the complexity of the fabrication procedure. Our work aims to reach a compromise between the detection efficiency of the device, and the cost and the simplicity of the fabrication protocol. Even though the sensitivity of our plasmonic nanostructures is lower than that reported in recent publications related to COVID-19 research (Masterson et al., 2021), our sensing platform is able to detect the presence of anti-SARS-CoV-2

antibody at clinically relevant concentration range in real samples. More importantly, in comparison with similar sensing devices, our fabrication protocol is simple and rapid, thus has higher potential for mass production.

Our previous work (Funari et al., 2020) has demonstrated the possibility of quantifying antibodies against the immobilized antigens in short time (i.e., 30 min) with relatively small sample volumes (i.e., 1 μL of serum) by integrating the LSPR substrate in a microfluidic channel and pumping the sample through the microfluidic chip by a syringe pump. Our future work aims to integrate the functionalized multiplexing sensor substrate developed in this work, with a microfluidic chip for higher throughput real-time screening analysis. Compared with other detection techniques such as the ELISA, microfluidic platform can introduce samples sequentially to sensing spots functionalized with different antigens, thus enable the detection of multiple targets in the same sample in a single experiment. We also plan to test our multiplex biosensing platform against samples produced with different immunization conditions, and real human samples from patients or vaccinated individuals in the future.

4. Conclusions

In this work, we have developed a multiplex nanoplasmonic sensing platform to discriminate the humoral response against 3 different antigens (Spike from SARS-CoV-2 and two different hemagglutinins (HAs) from influenza viruses). The antigens are immobilized on the sensing arrays by using a versatile strategy based on the streptavidin-biotin biomolecular interaction. This functionalization procedure requires only the presence of a biotin tag on the protein, therefore can be easily adapted to any desired combinations of antigens. Based on the principle of localized surface plasmon resonance (LSPR), the wavelength shift signifies the antibody binding activities with 3 representative monoclonal antibodies (mAb) with different selectivity. We further measure the humoral response in sera collected before and after immunization with the SARS-CoV-2 Spike protein, achieving responses in good agreement with the results obtained by the ELISA assay, verifying the production of antibodies in real samples by vaccination. Our multiplex assay has demonstrated multiple serum antibody profiling successfully, which can be easily expanded on a single chip to enhance the throughput by using the same fabrication protocols. To support the ongoing SARS-CoV-2 vaccine development without using expensive instruments or series of antibodies required for analysis, our ultimate goal is to establish a platform by combining the LSPR and microfluidics technologies, to quantify serum antibody levels against multiple antigens by a single minute dosage of serum samples.

CRediT authorship contribution statement

Riccardo Funari: Conceptualization, Sensing methodology, Funding acquisition, Data analysis, Writing the manuscript. **Hidehiro Fukuyama:** Protein methodology, Data analysis, Writing the manuscript. **Amy Q. Shen:** Conceptualization, Funding acquisition, Writing the manuscript.

Declaration of competing interest

The authors declare that they have no known competing financial interests or personal relationships that could have appeared to influence the work reported in this paper.

Acknowledgements

The authors thank Mr. Kang-Yu Chu from OIST for his contribution on the optical setup. Drs. Yoshinobu Okuno from OIPH for distribution of C179 hybridoma, Yoshimasa Takahashi from NIID for distribution of NSP2 hybridoma, Mikako Shirouzu and Takehisa Matsumoto from RIKEN BDR for providing recombinant C121 antibody, Drs. Chieko Okamura and Qingshun Lin from laboratory for lymphocyte differentiation RIKEN IMS for help of material preparations. R.F. acknowledges funding from the Japanese Society for the Promotion of Science (Grants-in-Aid for Early-Career Scientists, Grant # 20K20237). A.Q.S and H.F also thank seed funding from "SHINKA 2021 OIST".

Appendix A. Supplementary data

Supplementary data to this article can be found online at https://doi.org/10.1016/j.bios.2022.114193.

References

Ali, M.A., Hu, C., Jahan, S., Yuan, B., Saleh, M.S., Ju, E., Gao, S.-J., Panat, R., 2021. Adv. Mater. 33, 2006647.
Amanat, F., Stadlbauer, D., Strohmeier, S., Nguyen, T.H., Chromikova, V., McMahon, M., Jiang, K., Arunkumar, G.A., Jurczyszak, D., Polanco, J., et al., 2020. Nat. Med. 26, 1033–1036.
Antiochia, R., 2021. Biosens. Bioelectron. 173, 112777.
Bai, Y., Yao, L., Wei, T., Tian, F., Jin, D.-Y., Chen, L., Wang, M., 2020. JAMA 323, 1406.
Bhalla, N., Pan, Y., Yang, Z., Payam, A.F., 2020. ACS Nano 14 (7), 7783–7807. https://doi.org/10.1021/acsnano.0c04421.
Bian, S., Shang, M., Sawan, M., 2022. Biosens. Bioelectron. 114054.
Bray, R.A., Lee, J.-H., Brescia, P., Kumar, D., Nong, T., Shih, R., Woodle, E.S., Maltzman, J.S., Gebel, H.M., 2021. Transplantation 105, 79.
Burbelo, P.D., Riedo, F.X., Morishima, C., Rawlings, S., Smith, D., Das, S., Strich, J.R., Chertow, D.S., Davey Jr., R.T., Cohen, J.I., 2020. J. Infect. Dis. 222, 206.
Cady, N.C., Tokranova, N., Minor, A., Nikvand, N., Strle, K., Lee, W.T., Page, W., Guignon, E., Pilar, A., Gibson, G.N., 2021. Biosens. Bioelectron. 171, 112679.
Carter, L.J., Garner, L.V., Smoot, J.W., Li, Y., Zhou, Q., Saveson, C.J., Sasso, J.M., Gregg, A.C., Soares, D.J., Beskid, T.R., et al., 2020. ACS Cent. Sci. 6, 591.
Casadevall, A., Pirofski, L.-a., et al., 2020. J. Clin. Invest. 130, 1545.
Chauhan, G., Madou, M.J., Kalra, S., Chopra, V., Ghosh, D., Martinez-Chapa, S.O., 2020. ACS Nano 14, 7760.
Chen, H., Kou, X., Yang, Z., Ni, W., Wang, J., 2008. Langmuir 24, 5233.
Chen, P., Chung, M.T., McHugh, W., Nidetz, R., Li, Y., Fu, J., Cornell, T.T., Shanley, T.P., Kurabayashi, K., 2015. ACS Nano 9, 4173.
Dreyfus, C., Ekiert, D.C., Wilson, I.A., 2013. J. Virol. 87, 7149.
Drobysh, M., Ramanaviciene, A., Viter, R., Chen, C.-F., Samukaite-Bubniene, U., Ratautaite, V., Ramanavicius, A., 2022. Int. J. Mol. Sci. 23, 666.
Duan, X., Shi, Y., Zhang, X., Ge, X., Fan, R., Guo, J., Li, Y., Li, G., Ding, Y., Osman, R.A., et al., 2022. Biosens. Bioelectron. 199, 113883.
Dutta, N.K., Mazumdar, K., Gordy, J.T., 2020. J. Virol. 94.
Elledge, S.K., Zhou, X.X., Byrnes, J.R., Martinko, A.J., Lui, I., Pance, K., Lim, S.A., Glasgow, J.E., Glasgow, A.A., Turcios, K., et al., 2021. Nat. Biotechnol. 39, 928.
Fukuyama, H., Shinnakasu, R., Kurosaki, T., 2020. Immunol. Rev. 296, 132.
Funari, R., Chu, K.-Y., Shen, A.Q., 2020. Biosens. Bioelectron. 169, 112578.
Grossberg, A.N., Koza, L.A., Ledreux, A., Prusmack, C., Krishnamurthy, H.K., Jayaraman, V., Granholm, A.-C., Linseman, D.A., 2021. Nat. Commun. 12, 1.
Guo, L., Ren, L., Yang, S., Xiao, M., Chang, D., Yang, F., Dela Cruz, C.S., Wang, Y., Wu, C., Xiao, Y., et al., 2020. Clin. Infect. Dis. 71, 778.
Hartanto, H., Wu, M., Lam, M.L., Chen, T.-H., 2020. Biomicrofluidics 14, 061507.
Heaney, C.D., Pisanic, N., Randad, P.R., Kruczynski, K., Howard, T., Zhu, X., Littlefield, K., Patel, E., Shrestha, R., Laeyendecker, O., et al., 2021. medRxiv.
John Hopkins Center for Health Security, 2020. Global Progresses on Serology-Based Tests for Covid-19. URL. https://www.centerforhealthsecurity.org/resources/COVID-19/serology/Serology-based-tests-for-COVID-19.html. (Accessed 15 August 2020).
Kim, H., Lee, J.U., Song, S., Kim, S., Sim, S.J., 2018. Biosens. Bioelectron. 101, 96.
Koyama, T., Weeraratne, D., Snowdon, J.L., Parida, L., 2020. Pathogens 9, 324.
Kurt, H., Pishva, P., Pehlivan, Z.S., Özkan, E.G., Saleem, Q., Bayazıt, M.K., Yüce, M., 2021. Analytica Chimica Acta p 338842.
Lee, J.U., Nguyen, A.H., Sim, S.J., 2015. Biosens. Bioelectron. 74, 341.
Lee, J.-H., Lee, Y., Lee, S.K., Kim, J., Lee, C.-S., Kim, N.H., Kim, H.G., 2022. Biosens. Bioelectron. 203, 114034.
Liu, T., Hsiung, J., Zhao, S., Kost, J., Sreedhar, D., Hanson, C.V., Olson, K., Keare, D., Chang, S.T., Bliden, K.P., et al., 2020. Nature biomedical engineering 4, 1188.
Mas, S., Badran, A.A., Juárez, M.-J., de Rojas, D.H.F., Morais, S., Maquieira, Á., 2020. Biosens. Bioelectron. 166, 112438.
Masterson, A.N., Muhoberac, B.B., Gopinadhan, A., Wilde, D.J., Deiss, F.T., John, C.C., Sardar, R., 2021. Anal. Chem. 93 (25), 8754.
Matsuzaki, Y., Sugawara, K., Nakauchi, M., Takahashi, Y., Onodera, T., Tsunetsugu-Yokota, Y., Matsumura, T., Ato, M., Kobayashi, K., Shimotai, Y., et al., 2014. J. Virol. 88, 12364.
Mattioli, I.A., Castro, K.R., Macedo, L.J., Sedenho, G.C., Oliveira, M.N., Todeschini, I., Vitale, P.M., Ferreira, S.C., Manuli, E.R., Pereira, G.M., et al., 2022. Biosens. Bioelectron. 199, 113866.
Mayer, K.M., Hafner, J.H., 2011. Chem. Rev. 111, 3828.
Murphy, K., Weaver, C., 2016. Janeway's Immunobiology. Garland science.
Muruato, A.E., Fontes-Garfias, C.R., Ren, P., Garcia-Blanco, M.A., Menachery, V.D., Xie, X., Shi, P.-Y., 2020. Nat. Commun. 11 (1), 4059. https://doi.org/10.1038/s41467-020-17892-0.

Okuno, Y., Isegawa, Y., Sasao, F., Ueda, S., 1993. J. Virol. 67, 2552.
Oliveira, M.E., Lopes, B.V., Rossato, J.H.H., Maron, G.K., Gallo, B.B., La Rosa, A.B., Balboni, R.D.C., Alves, M.L.F., Ferreira, M.R.A., da Silva Pinto, L., et al., 2022. Surfaces 5, 187.
Orlov, A., Pushkarev, A., Znoyko, S., Novichikhin, D., Bragina, V., Gorshkov, B., Nikitin, P., 2020. Biosens. Bioelectron. 159, 112187.
Robbiani, D.F., Gaebler, C., Muecksch, F., Lorenzi, J.C., Wang, Z., Cho, A., Agudelo, M., Barnes, C.O., Gazumyan, A., Finkin, S., et al., 2020. Nature 584, 437.
Rodriguez-Moncayo, R., Cedillo-Alcantar, D.F., Guevara-Pantoja, P.E., Chavez-Pineda, O. G., Hernandez-Ortiz, J.A., Amador-Hernandez, J.U., Rojas-Velasco, G., Sanchez-Muñoz, F., Manzur-Sandoval, D., Patino-Lopez, L.D., et al., 2021. Lab Chip 21, 93.
Szunerits, S., Boukherroub, R., 2012. Chem. Commun. 48, 8999.
Theel, E.S., Slev, P., Wheeler, S., Couturier, M.R., Wong, S.J., Kadkhoda, K., 2020. J. Clin. Microbiol. 58, e00797.
Torrente-Rodríguez, R.M., Lukas, H., Tu, J., Min, J., Yang, Y., Xu, C., Rossiter, H.B., Gao, W., 2020. Matter 3, 1981.
Udugama, B., Kadhiresan, P., Kozlowski, H.N., Malekjahani, A., Osborne, M., Li, V.Y., Chen, H., Mubareka, S., Gubbay, J.B., Chan, W.C., 2020. ACS Nano 14, 3822.
U.S. Food and Drug Administration, 2020. EUA Authorized Serology Test Performance. URL. https://www.fda.gov/medical-devices/emergency-situations-medical-devices/eua-authorized-serology-test-performance. (Accessed 15 August 2020).
Valera, E., Jankelow, A., Lim, J., Kindratenko, V., Ganguli, A., White, K., Kumar, J., Bashir, R., 2021. ACS Nano 15 (5), 7899.
Willets, K.A., Van Duyne, R.P., 2007. Annu. Rev. Phys. Chem. 58, 267.
Wu, F., Zhao, S., Yu, B., Chen, Y.-M., Wang, W., Song, Z.-G., Hu, Y., Tao, Z.-W., Tian, J.-H., Pei, Y.-Y., et al., 2020. Nature 579, 265.
Wu, Y., Dang, H., Park, S.-G., Chen, L., Choo, J., 2022. Biosens. Bioelectron. 197, 113736.
Yakoh, A., Pimpitak, U., Rengpipat, S., Hirankarn, N., Chailapakul, O., Chaiyo, S., 2021. Biosens. Bioelectron. 176, 112912.
Zhai, P., Ding, Y., Wu, X., Long, J., Zhong, Y., Li, Y., 2020. Int. J. Antimicrob. Agents 55, 105955.
Zhang, Z., Wang, X., Wei, X., Zheng, S.W., Lenhart, B.J., Xu, P., Li, J., Pan, J., Albrecht, H., Liu, C., 2021. Biosens. Bioelectron. 181, 113134.
Zhao, J., Yuan, Q., Wang, H., Liu, W., Liao, X., Su, Y., Wang, X., Yuan, J., Li, T., Li, J., et al., 2020. Clin. Infect. Dis. 71, 2027.
Zhu, X., Wang, X., Han, L., Chen, T., Wang, L., Li, H., Li, S., He, L., Fu, X., Chen, S., et al., 2020. Biosens. Bioelectron. 166, 112437.
Žižek, S., 2020. Pandemic!: COVID-19 Shakes the World. John Wiley & Sons.